Chemical Engineering Journal 450 (2022) 138045

Contents lists available at ScienceDirect

Chemical Engineering Journal

journal homepage: www.elsevier.com/locate/cej

Impact of oxidants O_2, H_2O, and CO_2 on graphene oxidation: A critical comparison of reaction kinetics and gasification behavior

Zeng Liang [a], Rita Khanna [b], Kejiang Li [a,*], Feng Guo [c], Yan Ma [d], Hang Zhang [e], Yushan Bu [a], Zhisheng Bi [a], Jianliang Zhang [a]

[a] School of Metallurgical and Ecological Engineering, University of Science and Technology Beijing, Beijing 100083, PR China
[b] School of Materials Science and Engineering (ret.), The University of New South Wales, Sydney, NSW 2052, Australia
[c] School of Physical Science and Information Technology, Liaocheng University, Liaocheng 252000, PR China
[d] Max-Planck-Institut für Eisenforschung, Max-Planck-Straße 1, Düsseldorf 40237, Germany
[e] Modern Technology and Education Centre, North China University of Science and Technology, Tangshan, Tangshan 063009, PR China

ARTICLE INFO

Keywords:
Graphene surface
ReaxFF
H_2O
Gasification
Reaction kinetics

ABSTRACT

Fundamental understanding of the oxidation behavior of O_2, H_2O, and CO_2 in the process of oxyfuel combustion is of great significance. Extensive MD simulations with reactive force-field (ReaxFF) were performed to compare the gasification behavior under the individual influence of three oxidant molecules on a pristine and a mono-vacant graphene sheet. Distinct differences were observed in almost every aspect including initial kinetics, rate changes, complete/incomplete combustion, gasified regions, and the role of vacancy defects. In the case of O_2, the nucleation stage is harder while the later stages contained no limiting behavior; The gasification kinetics is highest for H_2O during initial periods, but the oxidative behavior changes as higher gas consumption levels are reached; CO_2 has the highest thermodynamic stability and the formation of stable intermediate structures troubles the gasification. Significant out-of-plane activity is observed in the case of H_2O oxidant. Results suggest that there may be little overlap in the oxidation sites for CO_2 and H_2O. In-depth atomic level investigations consistent with the experimental phenomenon will have implications for future design, process optimization, and their commercial application.

1. Introduction

Despite being the largest source of CO_2 emissions, coal continues to remain one of the biggest sources of power generation accounting for up to 32 % of the total power generated [1–3]. While cleaner energy sources may yet take several decades to develop and become commercially viable, coal industries in the developing and developed regions need to identify and incorporate less polluting and more efficient coal combustion technologies for their energy requirements [4]. Oxy-fuel combustion is one such promising low-carbon technology that has the potential to replace conventional air combustion of coals during power generation [5–7]. This approach requires the separation of oxygen from air and a partial mixing with a flue gas (a blend of CO_2 and steam) prior to injection into the coal boiler. The recirculation of flue gas within the furnace significantly increases CO_2 levels (60–70 vol%) in the furnace. The regenerated CO_2-rich flue gas can be easily compressed and stored away for reutilization [8], thereby greatly reducing the level of CO_2 emissions associated with power generation. Due to differences in the gas-phase characteristics such as heat capacity and radiant behavior, the simultaneous presence of O_2, H_2O, and CO_2 gases in the oxy-combustion environment can have a major influence on the overall coal combustion behavior. The focus of this study is to develop an in-depth fundamental understanding of the impacts of various oxidant gases on carbon gasification behavior, reaction kinetics, and mechanisms.

Under the oxy-fuel combustion process, CO_2 and H_2O gases have been known to affect the char structure, reactivity, and yield [9–11]. With flue gas recirculation, the CO_2 levels in the furnace gases are much higher in oxy-fuel combustion as compared to conventional, air-fired combustion. In a commercial operation, steam enrichment is the main byproduct of flue gas recycling; the steam concentration can vary from 5 vol% to 40 vol% [12,13]. Depending on the prior removal (or not) of the water vapor from flue gas, oxy-fuel combustion can be classified into dry recycle and wet recycle [14]. Even after moisture removal in a dry recycle, steam concentrations can be as high as 22 vol% [15]. In the wet

* Corresponding author at: 30 Xueyuan Rd., Haidian District, Beijing 100083, PR China.
E-mail address: likejiang@ustb.edu.cn (K. Li).

https://doi.org/10.1016/j.cej.2022.138045
Received 11 May 2022; Received in revised form 21 June 2022; Accepted 9 July 2022
Available online 14 July 2022

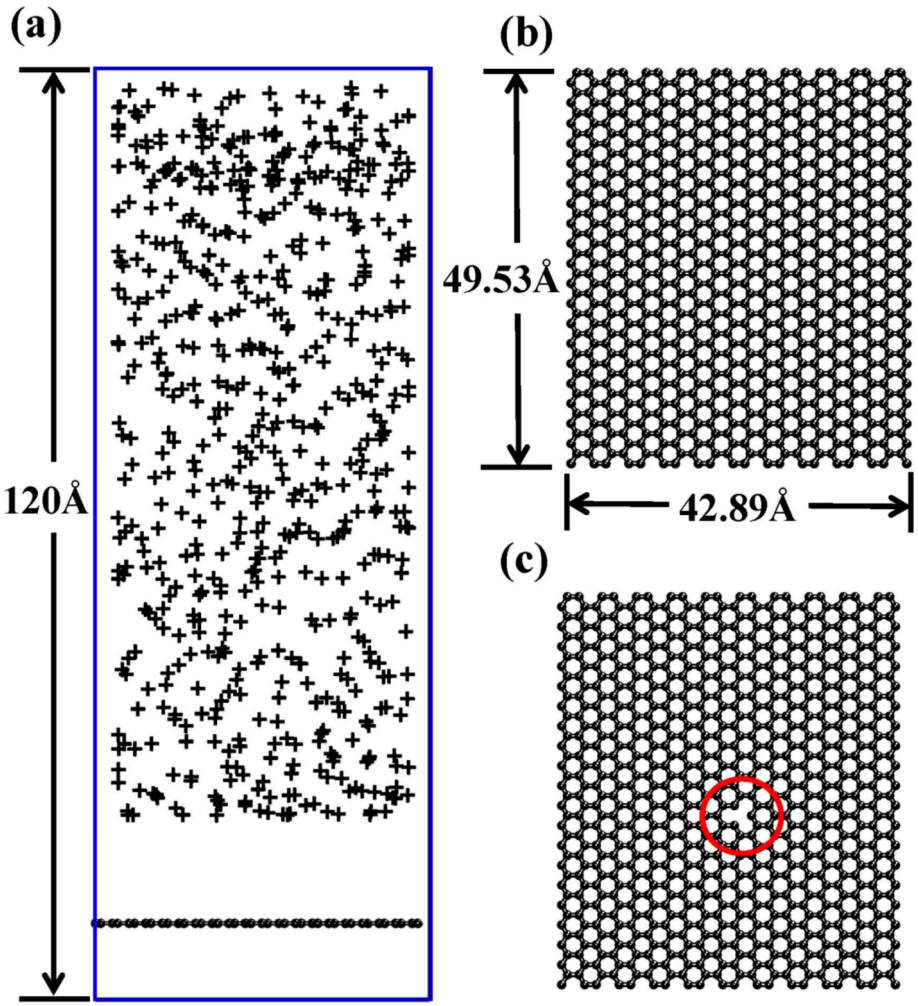

Fig. 1. Initial structure of graphene-oxidant gases reaction system: (a) positions of gaseous molecules '+' representing (O_2 or H_2O or CO_2) molecules in the simulation box; (b) positions of carbon atoms on a pristine graphene substrate; (c) carbon atom positions on graphene with a monovacancy. C atoms in the figure are marked in dark grey.

recycle, the steam levels can be as high as 37 vol%; however, the wet recycle oxy-fuel consumption has been determined to be economically more beneficial [16]. Combustion reactions under CO_2 can enhance the aromatization degree of coal and the generation of O-based functional groups affecting coal conversion and char reactivities [17]. The addition of H_2O in O_2/CO_2 mixtures has been seen to delay the ignition of coal particles and promote burnout and combustion reactivity [18]. Qing et al. [19] have reported on the isothermal evolution of char characteristics including structure and reactivity under (70 % CO_2; 30 % H_2O) using a thermo-gravimetric analyzer (TGA) in the temperature range 500–1000 °C. With gasification-associated weight losses starting at ~ 700 °C, the influence of H_2O was found to be stronger than CO_2 and resulted in higher char yields.

Several researchers have investigated the kinetics of char gasification at 800 °C and compared the gasification rate coefficients for CO_2 and H_2O with the corresponding rates for O_2 [20–22]. Kinetic rate coefficients with CO_2 and H_2O were found to be ~ 1–20 × 10^{-5} and 1–10 × 10^{-4} relative to the oxidation with O_2. Liu et al. [23] investigated gasification rates of three coal chars under steam and CO_2 atmospheres in the temperature range 1400–1800 K; the reaction rates under steam were found to be 2–3 times faster than CO_2 for all chars investigated. DeGroot and Richards [24] determined the gasification rates of a cellulose char at 800 °C in 0.1 atm of O_2, CO_2, and H_2O. The apparent activation energies for gasification reactions in O_2, CO_2, and H_2O were found to be 28.0, 66.8, and 38.1 kcal/mole respectively; corresponding reaction rates were determined to be 1.6 × 10^4, 1.0, and 18. These three oxidant gases are generally present in oxy fuels in a range of compositions and could influence the overall reaction kinetics and mechanisms. Roberts and Harris [25] have observed a competition as well as inhibition in the mixed atmosphere as the reactions for both H_2O and CO_2 were found to occur on the same active sites; the gasification rate in the mixed environment was found to be significantly lower than individual scenarios [26]. Some researchers have suggested that the oxidation reactions with H_2O and CO_2 occurred at different active sites [27,28]. Differences in coal rank, techniques used, and operating conditions can create additional issues while comparing reactivity results from different sources.

Mechanisms of the carbon gasification process have been extensively described by the classical Langmuir-Hinshelwood (L-H) theory [29]. As surface chemistry was found to be a critical factor influencing carbon reactivity [30], numerous studies have reported on graphene, a monolayer of carbon atoms in a hexagonal honeycomb structure, using computational quantum chemistry techniques [31,32]. Graphene-O_2 interactions are considered to be weak involving the dissociation of O_2 followed by the adsorption of O atoms at the vacancy sites [33]. Using density functional theory (DFT), the particular adsorption preference of CO_2 chemisorption on the zigzag edge carbon sites for isolated carbene-like zigzags was found[34]. DFT has also been used for identifying differences between H_2O and CO_2 adsorption at defect sites; the reaction of H_2O was found to involve its rotation and slow adsorption at the defect

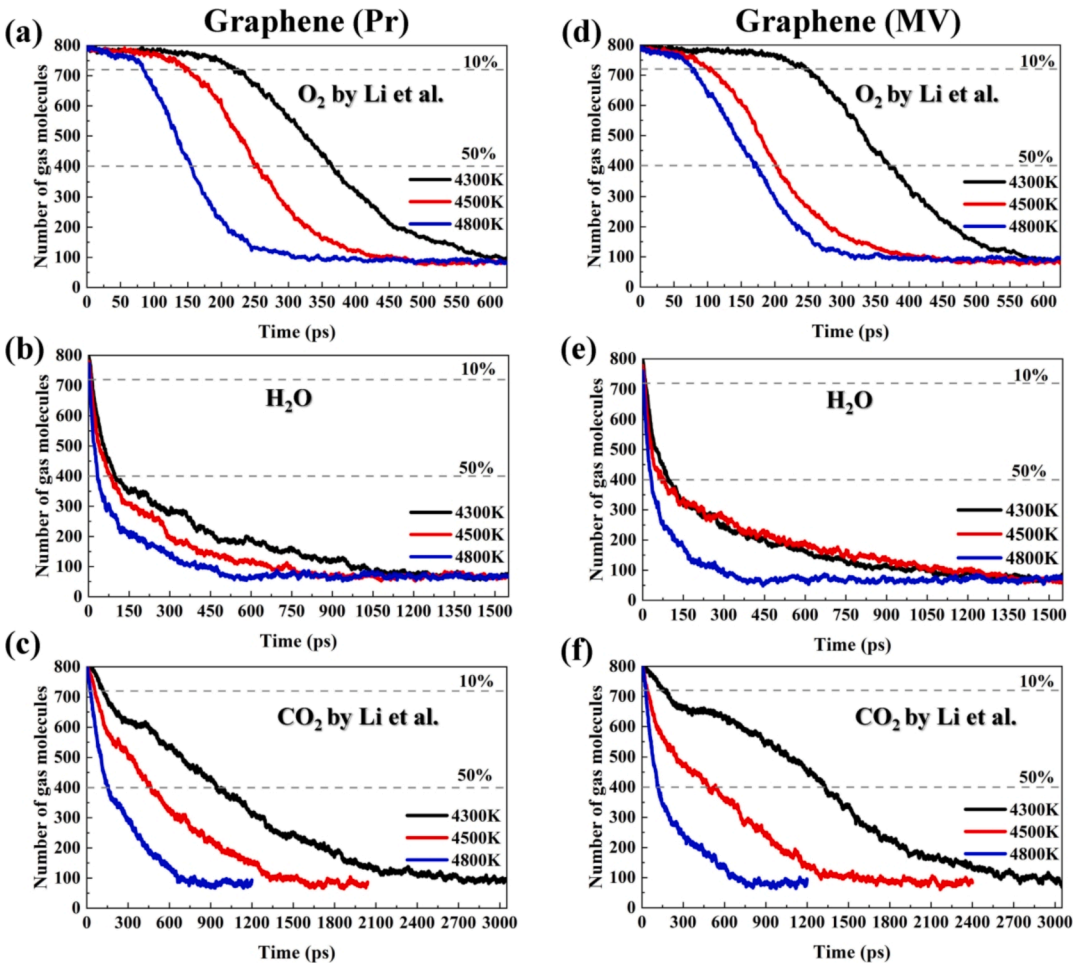

Fig. 2. Consumption of oxidant molecules as a function of time in Pr and MV graphenes. Data has been presented for O_2, H_2O, and CO_2 gases at three temperatures. Data for O_2 and CO_2 were from our previous studies [37,38].

site [35]. Zhao et al. [36] have suggested that the higher gasification efficiency with H_2O could be attributed to H atoms promoting desorption by reducing the aromaticity of edge carbon structure. An in-depth understanding of the key differences between the three oxidants including atomic-scale features of gasification reactions, influence of reaction temperature, reaction times, defects, etc. is presently very limited. A fundamental investigation is therefore required for a deeper perspective on the optimal choice and relative proportions of oxidants for future advances in power generation.

In this study, extensive atomic-scale ReaxFF-MD simulation studies on the interaction of graphene with H_2O over a wide temperature range for long periods of reaction times were reported and compared with the interaction with O_2 and CO_2 published in our previous studies [37,38]. Two types of graphenes were used in these simulations: defect-free pristine structure (Pr) and the presence of a mono vacancy (MV). The focus of these studies is to identify key differences in the carbon gasification behavior with three oxidants in terms of reaction kinetics, degree of oxidation, the influence of temperature, time, and the presence of vacancy defects. This study is expected to provide a fundamental understanding towards establishing guidelines for effective control of graphene gasification with O_2, H_2O, and CO_2. These simulations were carried out separately for each gas and will be extended to gas mixtures in the near future.

2. Molecular dynamics computer simulations

The large-scale atomic/molecular massively parallel simulator (LAMMPS)[39] code in conjunction with the reactive force-field (ReaxFF) method was used to perform molecular dynamics simulations. A general bond-order dependent potential system was used to simulate bond breaking and bond formation in hydrogen-carbon–oxygen systems [40]. ReaxFF potentials have previously been used for computing reaction pathways, kinetics, transition states, and process energetics [39,41,42]. These simulations were generally in good agreement with quantum mechanical computations as well as experimental data. ReaxFF parameter sets based on potentials reported by Castro-Marcano et al. [43] and Weismiller et al. [44] were used in the present study. Non-bonded Coulomb and van der Walls interactions were computed for every atomic pair individually over a long range; a shielding term was used for curbing extreme close-range interactions.

Similar to our previous studies [37,38], simulations were carried out in the canonical NPT ensemble on a 42.89 Å × 49.53 Å pristine graphene sheet (Pr) containing 800 carbon atoms. Simulations were also carried out on a graphene sheet containing a monovacancy (MV) in the central region. Conjugate gradient methods were used for geometry optimization and energy minimization and were followed by relaxation at 300 K for 20 ps. Additional studies were also carried out at 4000 K, 4400 K and 4800 K for 500 ps. While minimal changes were observed in the basal plane, out-of-plane carbon movements were typical of thermal vibrations (see **Fig. S1**). Oxidation simulations were carried out in the canonical NVT ensemble. The graphene sheet was placed in a lower region of a simulation box with x and y dimensions corresponding to the size of the relaxed graphene sheet and a height of 120 Å. A large number of H_2O molecules were distributed randomly above the graphene sheet, which

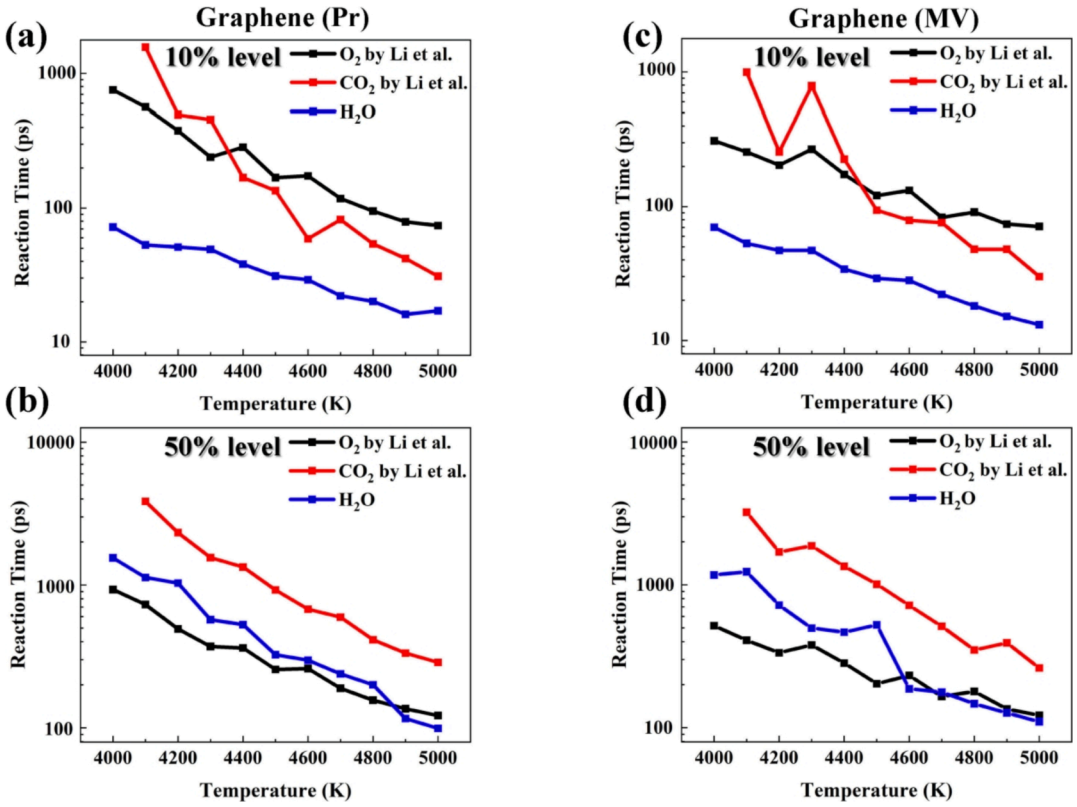

Fig. 3. Time taken for reaching 10% and 50% gas consumption levels at a function of temperature. A logarithmic scale has been used along the y-axis due to the wide data range. Data for O_2 and CO_2 were from our previous studies [37,38].

differed from the previous work[37,38] by the oxidant used; 800 H_2O oxidant molecules were used in this case as well for sake of comparison with previous studies. A single type of oxidant molecule was used in individual simulations and there was no mixing of different oxidants during simulations. Reflecting walls were adopted along the z-direction to constrain oxidant molecules within the simulation box. Periodic boundary conditions were used in the × and y directions to eliminate the influence of edge effects. Four corner carbon atoms on the graphene sheets were pinned to prevent lateral motion along the z-axis. A schematic representation of the simulation cell is shown in Fig. 1.; the symbol '+' in Fig. 1a has been used to represent 'O_2' or 'H_2O' or 'CO_2' molecule depending on the oxidant gas being investigated. Simulation cells for these three gases with appropriate molecular structures have been shown in **Fig. S2**.

MD simulations were carried out in the temperature range 4000 K to 5000 K. The oxidation kinetics were generally quite slow below 4000 K requiring excessive (>5000 ps) simulation times. Such simulations were neither practical nor feasible in view of high computing costs [45,46].

Nosé–Hoover thermostat was used for temperature control. Starting initially from 300 K, target simulation temperatures could generally be achieved within 30 ps. Oxidation behavior was observed for times up to 2000 ps; the evolution of all requisite system parameters was recorded. A time step of 0.1 fs ensured a high precision mapping of the oxidation process. Output data files containing the concentrations of different species and oxidation products were recorded every thousand time-steps. All simulations were repeated at least three times at each temperature investigated to ensure the overall reproducibility of MD simulations.

3. Results

3.1. Oxidation kinetics

Three key variables used in these simulations were: the type of oxidant gas used, temperature, and defect status (pristine or mono-vacant graphene structure). Fig. 2 shows the kinetics of oxidant (O_2, H_2O, and CO_2) consumption for Pr and MV graphenes. Although data were collected at several temperatures in the 4000–5000 K range, data from three representative values 4300 K, 4500 K, and 4800 K have been plotted in this figure for comparing various trends. Initial molecular concentration was chosen as 800 molecules for all three gaseous species. Additional gas data for H_2O molecules have been provided in the supplementary **Fig. S3**; corresponding data for CO_2 and O_2 can be found elsewhere [37,38].

In the case of O_2 gas, there was negligible consumption of oxidant in the initial times as indicated by rather flat curves. These flat regions ranged between 150 ps (4300 K) and 80 ps (4800 K) for Pr graphene; the corresponding range for MV graphene was 180 ps (4300 K) to 60 ps (4800 K). No such initial regions were observed in the case of H_2O and CO_2 oxidants for both graphenes. The consumption of these oxidant molecules started immediately with the onset of reaction time, albeit with significant differences in their initial reaction kinetics. Reaction kinetics was very rapid for H_2O molecules and relatively slower for CO_2. The rate of molecular consumption was found to generally increase with increasing temperatures; this trend was observed for all three gases for both Pr and MV graphenes.

Fig. 3 shows the times taken for the consumption of 10 % and 50 % oxidant molecules for temperatures ranging between 4000 K and 5000 K. A logarithmic scale has been used on the y-axis due to the wide range of observed reaction times. With times ranging between 20 and 80 ps, the initial 10 % consumption of H_2O molecules was very rapid and fastest for both graphenes over the entire thermal range investigated.

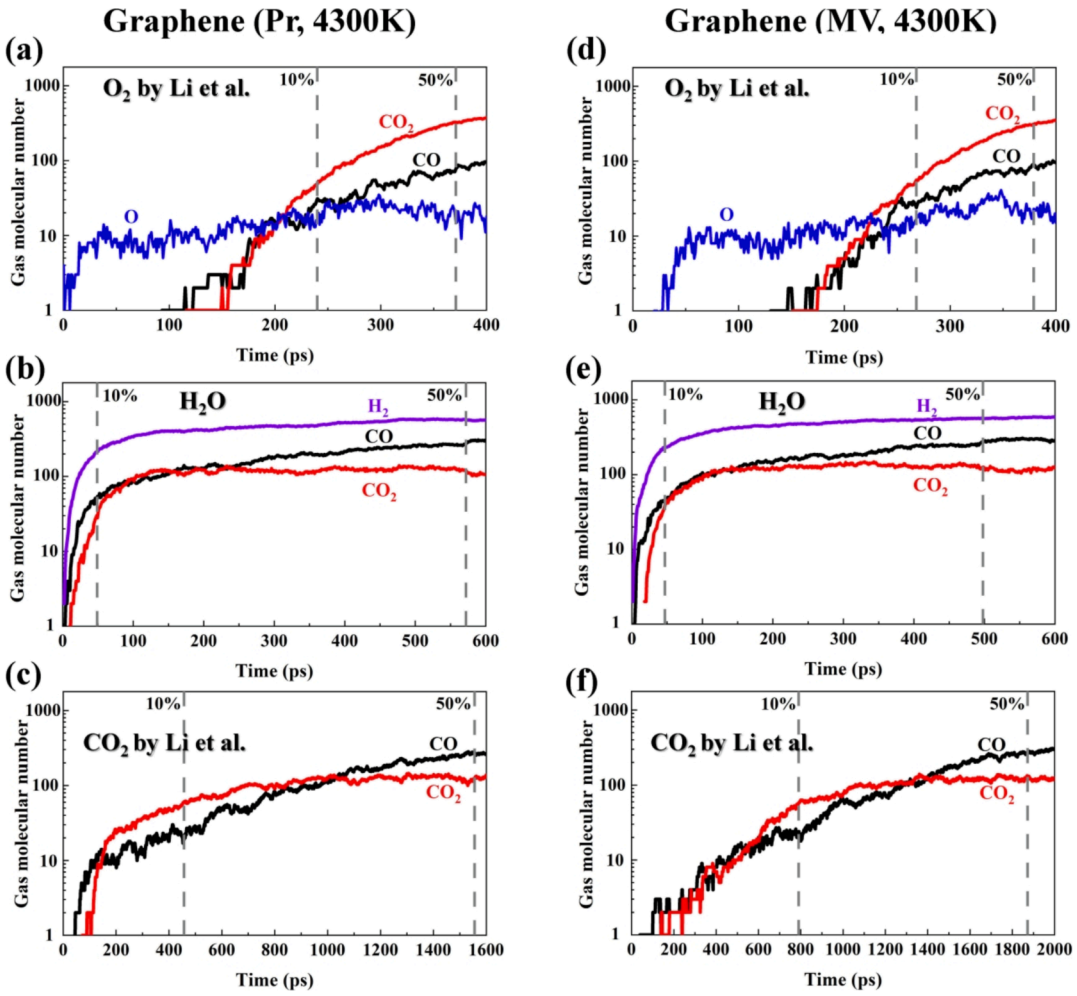

Fig. 4. Gas generation data (O, H_2, CO, and CO_2) as a function of time. Results for the three oxidants have been shown for gasification at 4300 K. Data for O_2 and CO_2 were from our previous studies [37,38].

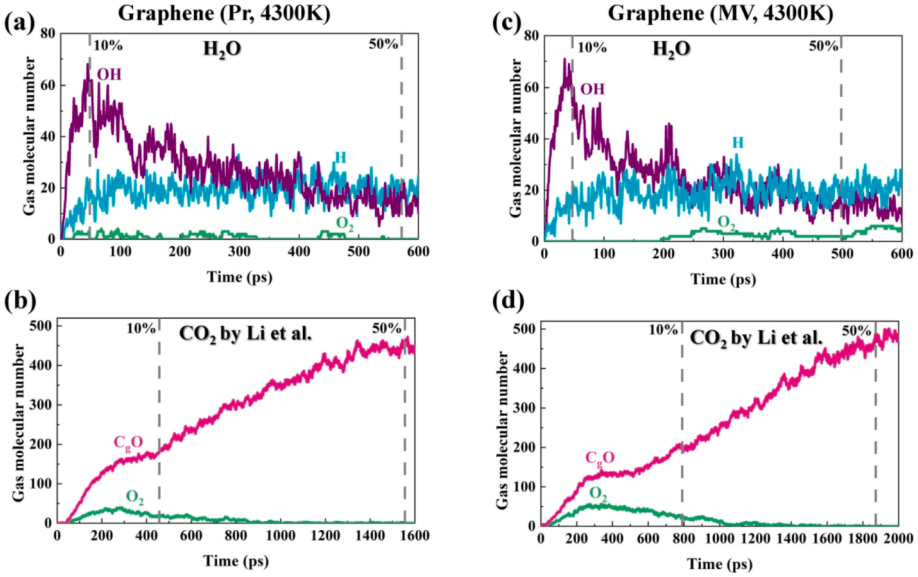

Fig. 5. Generation data for additional gases/molecules (OH, H, C_8O, and O_2) as a function of time. Results for the three oxidants have been shown for gasification at 4300 K. Data for CO_2 were from our previous studies [37,38].

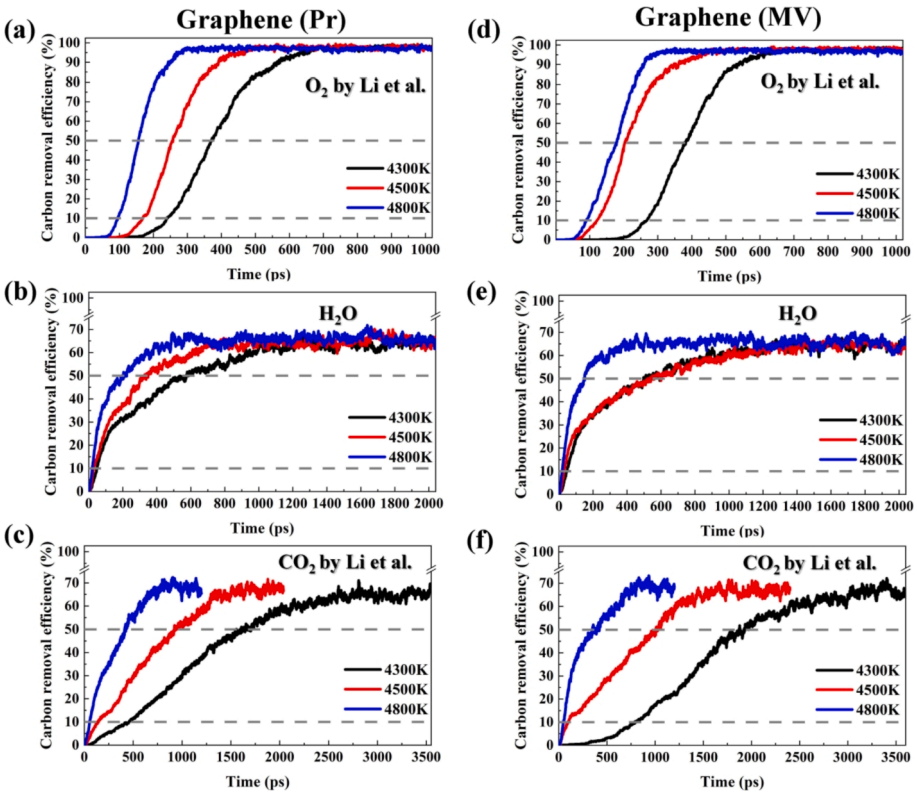

Fig. 6. Carbon removal efficiency (%) as a function of time for the three oxidants at 4300 K, 4500 K, and 4800 K. Data has been shown for Pr and MV graphenes. Data for O_2 and CO_2 were from our previous studies [37,38].

The kinetics of O_2 consumption was faster than the corresponding rates for CO_2 up to ~ 4500 K; this trend was however seen to reverse at higher temperatures. These results were observed for both graphenes with times ranging between 200 to over 1000 ps. However, at the 50 % consumption level, the kinetics was fastest for O_2 followed by H_2O and then CO_2 thereby pointing to significant changes in the oxidation behavior with the progress of the oxidation reaction.

3.2. Gas generation

Fig. 4 and Fig. 5 show the evolution of gas molecules during graphene oxidation with the three oxidants. Representative data has been plotted for the 4300 K simulation results. Results for O, H_2, CO, and CO_2 molecules have been shown in Fig. 4; the release of additional molecules OH, H, C_gO (representing CO produced from the dissociation of the oxidant gas CO_2) and O_2 are shown in Fig. 5. Dotted reference lines have been drawn to represent 10 % and 50 % oxidant consumption levels. In the case of O_2, small amounts of dissociated 'O' atoms were observed within a few ps of reaction time; these numbers however hovered around 10 for times over 400 ps without much change. The generation of CO and CO_2 gas molecules started at ~ 150 ps; CO_2 levels were found to be higher than CO at 10 % and 50 % oxygen consumption. These trends were observed for both Pr and MV graphenes.

The results were significantly different in the case of the oxidant H_2O. There was a rapid initial generation of H_2 gas reaching ~ 300 molecules within 50 ps and tending to flatten out at later times. There was little change in H_2 numbers between 10 % and 50 % H_2O consumption levels. Higher levels of CO were produced initially but these were overtaken by CO_2 at later times. A number of other molecules, OH, H, C_gO, and small amounts of O_2 were also detected in the reaction products (Fig. 5). Results for Pr and MV graphene were found to be quite similar. In the case of the oxidant CO_2, CO and CO_2 were the two key reaction products. Initially, CO_2 levels were somewhat higher than CO levels, but this trend was reversed at later times and higher oxidant consumption. Small amounts of O_2 were also detected.

3.3. Gasification efficiency

The carbon removal (gasification) efficiency (%) was computed as: (No. of C atoms removed/ initial no. of C atoms) × 100. The results for the three oxidants have been plotted in Fig. 6 for 4300 K, 4500 K, and 4800 K. Dotted lines have been drawn to indicate 10 % and 50 % carbon removal levels. In the case of O_2, after a slow initial start, carbon removal occurred rapidly reaching efficiency levels in excess of 95 %. The reaction kinetics was fastest at 4800 K followed by 4500 K and 4300 K. Both Pr and MV graphenes showed similar trends. In the case of H_2O, gasification started almost immediately but could only reach ~ 65 % efficiency even after extended periods. While the reaction was rapid during the initial 200–400 ps, it tended to flatten out at later times. In the case of Pr graphene, the reaction kinetics was highest for 4800 K followed by 4500 K and 4300 K. However, similar levels of reaction kinetics were observed at 4300 K and 4500 K for MV graphene. The rates for the carbon removal efficiency were relatively slow for CO_2 gas taking longer reaction times. In the case of CO_2 as well, the carbon removal efficiency was found to flatten out ~ 65 % level. Corresponding results in terms of the number of C atoms gasified have been presented in the supplementary **Fig. S4**.

3.4. Apparent kinetics analysis for gasification

The kinetic fit of the normalized gasification C number [47,48] was performed using the Avrami–Erofeev equation[38,49,50], combined with the Arrhenius equation[51] to plot the apparent activation energy of the carbon gasification reaction in the H_2O case, see Fig. 7.

$$\int k \cdot dt = \int \frac{dx}{f(x)} = \sqrt{-\ln(1-x)} \tag{1}$$

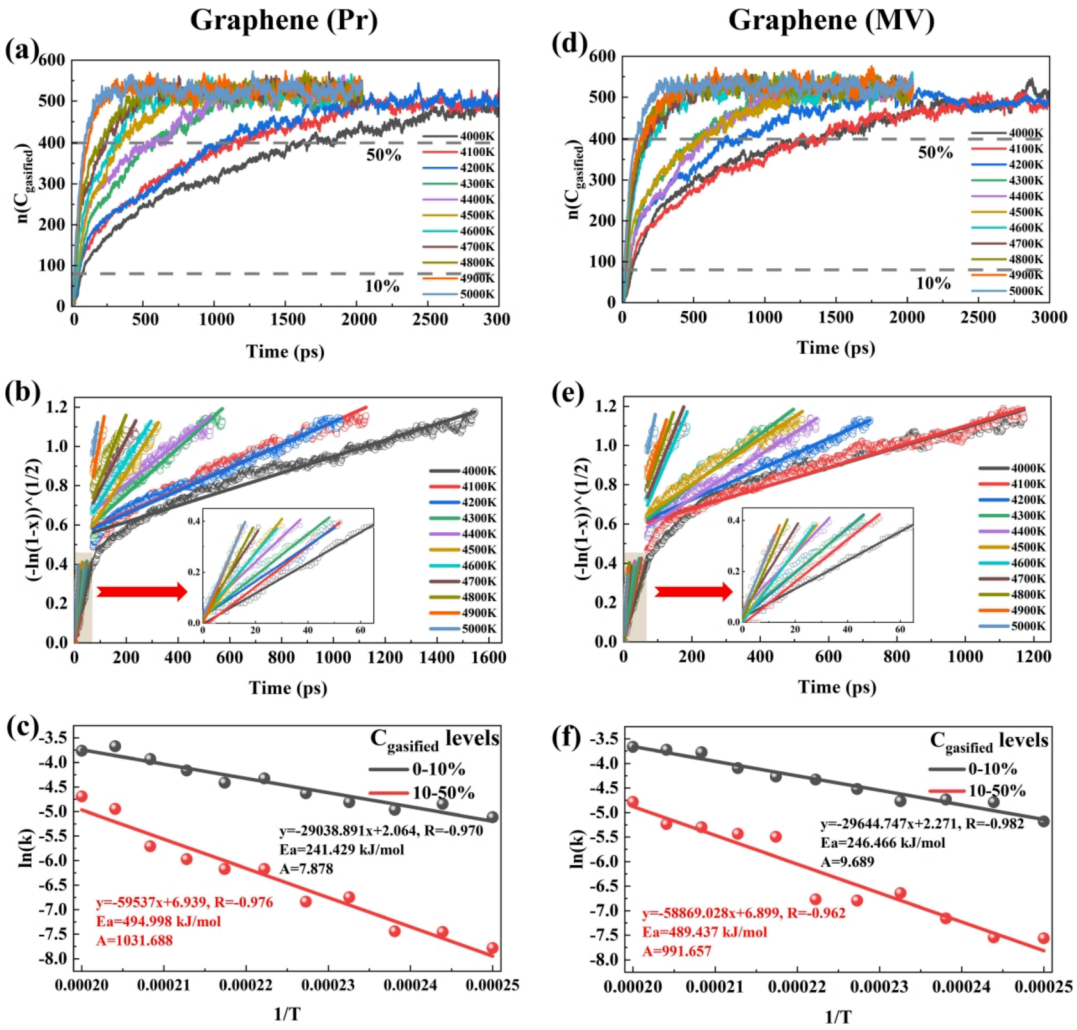

Fig.7. Mathematical fitting to get the kinetic parameters: (a), (d) evolution of the number of gasified carbon atoms with time (b), (e) fitting between the value of $\sqrt{-\ln(1-x)}$ with time to get the reaction constant; (c), (f) fitting between ln(k) with 1/T to get the kinetic parameters; for pristine graphene (Pr) and mono-vacancy graphene (MV) respectively.

$$\ln(k) = \ln(A) - \frac{E}{RT} \tag{2}$$

of which, x, t (ps), k, A, E, R, and T are the degree of conversion, time, a temperature-dependent rate constant, the pre-exponential factor (ps^{-1}), the activation energy ($kJ{\cdot}mol^{-1}$), the gas constant (8.314 $J{\cdot}mol^{-1}{\cdot}K^{-1}$) and the temperature (K), respectively.

The carbon gasification level was divided into two stages (0–10 %, 10 %-50 %), and the apparent activation energy results were obtained: Pr, 241.429 kJ/mol, 494.998 kJ/mol; MV, 246.466 kJ/mol, 489.437 kJ/mol. Corresponding activation energies for the other two oxidants are: O2 (Pr: 225.4 kJ/mol, MV: 182.7 kJ/mol); CO2 (Pr: 371.6 kJ/mol, MV: 343.2 kJ/mol) [37,38]. The apparent activation energy at the initial stage of the reaction is in good agreement with the experimental value (190–270 kJ/mol) of steam gasification of coal, coke, commercial graphite, *etc.* which contains a large number of active sites. However, as the reaction progresses, significant changes in the oxidation behavior occur. The apparent activation energy for the evolution of the gasification level from 10 % to 50 % doubles compared to the initial stage.

3.5. Nucleation and growth of gasified regions

Detailed results on the evolution of gasified regions under the individual influence of the three oxidants (4300 K) are presented in Fig. 8. Results for Pr and MV graphenes have been presented for the carbon gasification levels of 10 % and 20 %. In the case of O_2 gas, a single gasified region was observed in the middle of the simulation cell of Pr graphene at the 10 % gasification level. This single region had grown bigger at the 20 % gasification level; additional nucleation/gasification sites were not observed. However, for the MV graphene, two gasification regions were observed at the 10 % level; these had grown further to merge into one region at the 20 % level. In the case of H_2O, two large gasification regions were observed for Pr graphene at the 10 % level. These had grown much bigger in size at the 20 % level of carbon gasification. Three distinct regions were observed for the MV graphene at the 10 % level and also found to increase in size at the 20 % level. In the case of CO_2 gas, relatively smaller gasification regions were observed that tended to grow at higher gasification levels. It is curious to note that at the 10 % carbon consumption level, the region around the vacancy was not gasified.

A local map of the reaction mechanism of the enlarged oxidized region caused by the erosion of the carbon surface edge by oxygen is also plotted, see Supplementary **Fig. S5**. The atomic motion behavior captured using the Reaxff molecular dynamics simulations is in high agreement with the DFT calculations of Oyarzún *et al.*[35,52] In addition, the surface saturation mechanism during the simulation at low temperature was also recorded, see Videos 1 and 2 in the Supplementary Material, corresponding to the formation and saturation of single- and

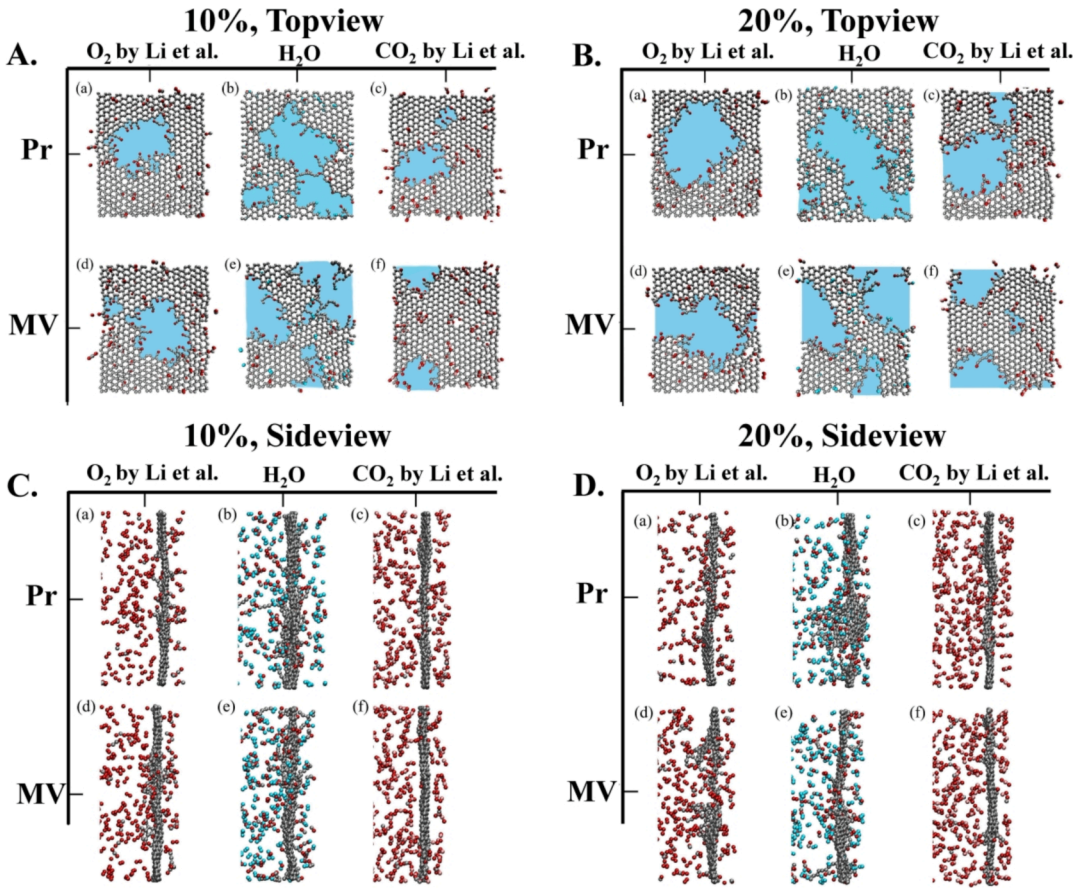

Fig. 8. Atomistic mapping of graphene oxidation under the individual influence of O_2, H_2O, and CO_2 oxidants at 4300 K. Gasified regions (marked in blue) have been shown for Pr and MV graphenes at the carbon gasification levels of 10 % and 20 %. Both top (A, B) and slightly magnified side views (C, D) of graphene sheets are shown for a ready reference. Data for O_2 and CO_2 were from our previous studies [37,38]. C atoms in the figure are marked in dark grey. The C, H, and O atoms in the figure are marked with dark gray, cyan, and red, respectively. In the case of CO_2 as the oxidant, the C atoms in the gas are distinguished by pink.

double-vacancy defects on the graphene surface, respectively.

4. Discussion

Extensive results have been presented on the graphene gasification behavior under the individual influence of O_2, H_2O, and CO_2 oxidant gases. Significant differences were observed in their reaction kinetics and consumption as a function of time. While the consumption of H_2O and CO_2 started instantaneously at the start of the gasification reaction, there was a time delay in the case of O_2 gas. This result indicates that the nucleation stage was somewhat harder in the case of O_2, whereas no such difficulty was observed for H_2O and CO_2 gases. Once initiated, the oxidation with O_2 was found to be very rapid indicating no limiting behavior during later stages. The gasification kinetics was highest for H_2O during initial periods; a 10 % gas consumption level was achieved within 100 ps in the temperature range 4000–5000 K for both graphenes. But this gasification rate slowed down considerably at later times; up to 100–1000 ps were required to achieve 50 % gas consumption levels. The initial region was accompanied by an extensive release of H_2 gas. The generation of OH, H, and O_2 was also detected. While complete combustion was observed with O_2, both H_2O and CO_2 showed an incomplete combustion behavior attributed to a certain extent to the insufficient supply of oxygen [53,54].

Fig. 9a and 9c show the number of H_2 molecules generated as a function of time from Pr and MV graphenes at 4300 K, 4500 K, and 4800 K. All plots show a very sharp release of H_2 molecules within the first 100 ps. Up to 300 to 500 H_2 molecules were produced during this period. This result is also reflected in the H_2 generation rates plotted in Fig. 9b and 9d. Up to 12 H_2 molecules/ps were produced at 4800 K, 8 molecules/ps for 4500 K, and 6 molecules/ps at 4300 K; similar trends were observed for both graphenes. The production of H_2 tended to slow down at longer times suggesting a change in the reaction mechanism. These results are in good agreement with published results on coal steam gasification [55,56].

During oxidation with CO_2, the key reaction products were CO and CO_2 gases. A significant proportion of CO gas (C_gO) was from the dissociation of CO_2; a small amount of O_2 was also released in the process [$CO_2 \rightarrow C_gO + O$]. The presence of a monovacancy had a negligible influence on oxidation with CO_2 during initial times. These can be attributed to the high thermodynamic stability of CO_2 and slow char gasification through the forward Boudouard reaction ($C + CO_2 \rightarrow 2CO$) [57,58]. Gasification rates were found to be substantially lower in the initial region due to the formation of relatively stable intermediate structures. The presence of a monovacancy promoted reaction kinetics only at relatively low temperatures with little influence at higher temperatures [37].

In Fig. 8, a wide variation was observed in the sizes of gasified regions (shown in 'blue') for the three oxidants after the removal of 10 % and 20 % carbons. This apparent difference was caused by the out-of-plane movement of C atoms. Taking a closer look at the side-views in Fig. 8C and 8D, it can be seen that there was very little out-of-plane movement during oxidation with CO_2 gas; fairly narrow and straight graphene planes can be observed for 10 % and 20 % C removal scenarios in Pr and MV graphenes. Significant out-of-plane activity can be seen in the case of H_2O gas with a relatively thicker graphene sheet, especially seen for 20 % C removal from Pr graphene. These movements can make

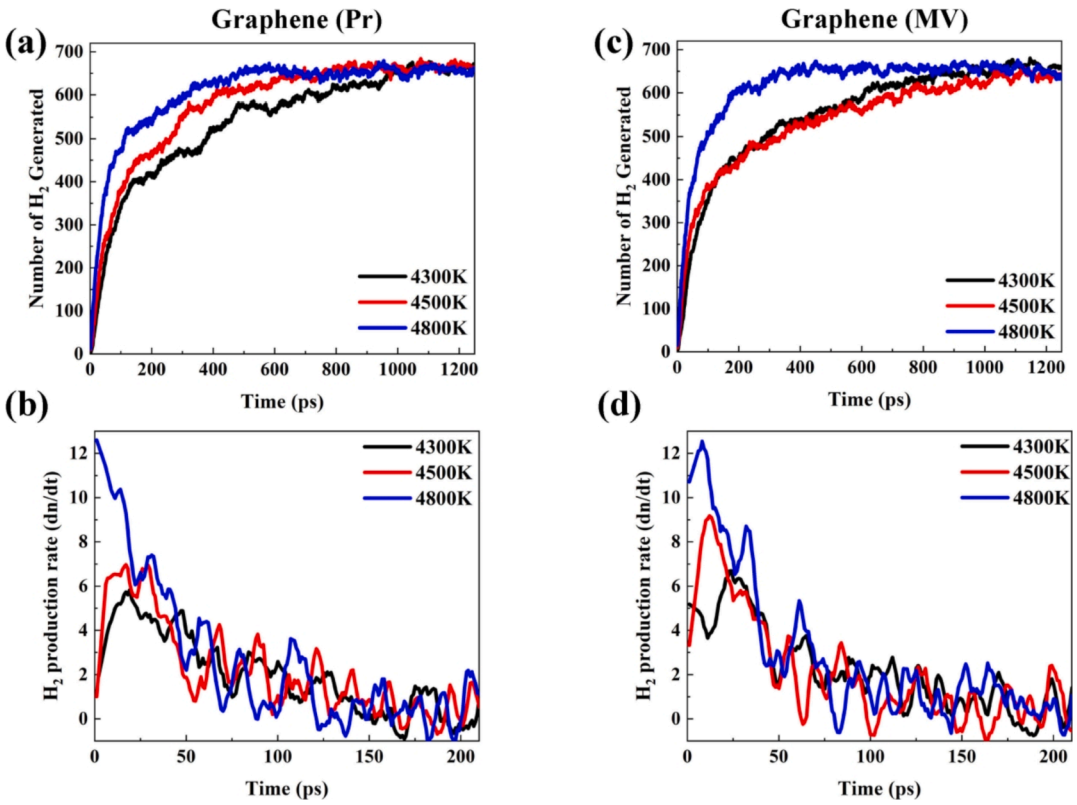

Fig. 9. The number of H_2 molecules generated as a function of time for (A) Graphene (Pr) and (B) Graphene (MV). Corresponding H_2 generation rates are shown in (C) and (D) respectively. Data has been presented for 4300 K, 4500 K, and 4800 K in all plots.

the oxidized regions larger in size. An intermediate behavior was observed with O_2 gas. These results also suggest that there may be little overlap in the oxidation sites for CO_2 and H_2O. Our results indicate that the oxidation with CO_2 and H_2O may not be occurring on the same active sites [25–27].

Following compositions of gas mixtures have been reported in the Callide oxyfuel project: Air mode: 4.5 vol% O_2, 15.0 vol% CO_2 and 8 vol % H_2O; Recycled flue gas: 6.8 vol% O_2, 59.9 vol% CO_2 and 20.5 vol% H_2O; Oxy firing mode: 5.4 vol% O_2, 72.2 vol% CO_2 and 21.6 vol% H_2O [59]. A detailed gasification behavior of three individual oxidant gases has been reported in this study. When present as mixtures, there is a strong likelihood of significant differences in their oxidation behavior, thus making the prediction of the overall behavior challenging. Based on the fundamentals developed in this study, our future studies will be on the gasification behavior of oxidant gas mixtures for application in commercial and real-life applications.

5. Conclusions

In-depth atomic level investigations were reported on the gasification behavior of graphenes with three oxidants (O_2, H_2O, and CO_2) gases under similar operating conditions. Significant differences were observed in almost every aspect of their carbon gasification behavior including initial kinetics of gas consumption and carbon removal, rate changes at later times, complete/incomplete combustion, the geometry of gasified regions, and the role of vacancy defects. The overall gasification behavior and the kinetics of O_2, H_2O, and CO_2 were found to be quite different at every stage of the reaction process. While the behavior of gas mixtures in a commercial scenario is unlikely to be a linear combination or extension of individual gases, this study has laid the foundations for their behavior at an atomic scale. This valuable knowledge is expected to play a key role in the future design, process optimization of low carbon technologies, and reducing the carbon footprint of coal-based power generation.

CRediT authorship contribution statement

Zeng Liang: Data curation, Formal analysis, Manuscript writing. **Rita Khanna:** Draft plan and draft manuscript. **Kejiang Li:** Conceptualization, Simulation, Discussion, Review & Editing. **Feng Guo:** Software. **Yan Ma:** Manuscript revision, discussion. **Hang Zhang:** Software. **Yushan Bu:** Software, Visualization. **Zhisheng Bi:** Visualization. **Jianliang Zhang:** Investigation, Supervision, Funding acquisition.

Declaration of Competing Interest

The authors declare that they have no known competing financial interests or personal relationships that could have appeared to influence the work reported in this paper.

Data availability

Data will be made available on request.

Acknowledgements

The authors acknowledge the financial support from the Young Elite Scientist Sponsorship Program by CAST (YESS20210090), the National Natural Science Foundation of China (51974019, 51804025), and the National Key Research and Development Program of China (2017YFB0304300&2017YFB0304303). The authors acknowledge Prof. Dierk Raabe from the Max-Planck-Institut für Eisenforschung for his guidance on this work. Computations were completed on the Niagara supercomputer at the SciNet HPC Consortium in the Compute/Calcul Canada national computing platform. SciNet is funded by the Canada Foundation for Innovation under the auspices of Compute Canada, the

Government of Ontario, Ontario Research Fund - Research Excellence, and the University of Toronto. The authors acknowledge Prof. Mansoor Barati of the University of Toronto for the technical support.

Appendix A. Supplementary data

Supplementary data to this article can be found online at https://doi.org/10.1016/j.cej.2022.138045.

References

[1] IEA, Coal-Fired Power, 2021. https://www.iea.org/reports/coal-fired-power.
[2] Q. Du, X. Liu, E. Wang, S. Wang, Strength Reduction of Coal Pillar after CO2 Sequestration in Abandoned Coal Mines, Minerals 7 (2) (2017) 26.
[3] IEA, Global Energy & CO2 Status Report 2019, 2019. https://www.iea.org/reports/global-energy-co2-status-report-2019.
[4] Z. Zhang, Z. Zhao, F. Wu, C. Luo, X. Li, Y. Chen, B. Lu, L. Zhang, C. Zheng, Reaction behaviors of a single coal char particle affected by oxygen and steam under oxy-fuel combustion, Fuel 291 (2021), 120229, https://doi.org/10.1016/j.fuel.2021.120229.
[5] C. Zheng, Z. Liu, J. Xiang, L. Zhang, S. Zhang, C. Luo, Y. Zhao, Fundamental and Technical Challenges for a Compatible Design Scheme of Oxyfuel Combustion Technology, Engineering 1(1) (2015) 139-149. 10.15302/J-ENG-2015008.
[6] T. Wall, Y. Liu, C. Spero, L. Elliott, S. Khare, R. Rathnam, F. Zeenathal, B. Moghtaderi, B. Buhre, C. Sheng, R. Gupta, T. Yamada, K. Makino, J. Yu, An overview on oxyfuel coal combustion—State of the art research and technology development, Chem. Eng. Res. Des. 87 (8) (2009) 1003–1016, https://doi.org/10.1016/j.cherd.2009.02.005.
[7] L. Chen, S.Z. Yong, A.F. Ghoniem, Oxy-fuel combustion of pulverized coal: Characterization, fundamentals, stabilization and CFD modeling, Prog. Energy Combust. Sci. 38 (2) (2012) 156–214, https://doi.org/10.1016/j.pecs.2011.09.003.
[8] E.S. Hecht, C.R. Shaddix, M. Geier, A. Molina, B.S. Haynes, Effect of CO2 and steam gasification reactions on the oxy-combustion of pulverized coal char, Combust. Flame 159 (11) (2012) 3437–3447, https://doi.org/10.1016/j.combustflame.2012.06.009.
[9] T. Li, L. Zhang, L. Dong, P. Qiu, S. Wang, S. Jiang, C.-Z. Li, Changes in char structure during the low-temperature pyrolysis in N2 and subsequent gasification in air of Loy Yang brown coal char, Fuel 212 (2018) 187–192, https://doi.org/10.1016/j.fuel.2017.10.026.
[10] J. Xu, S. Su, Z. Sun, M. Qing, Z. Xiong, Y. Wang, L. Jiang, S. Hu, J. Xiang, Effects of steam and CO2 on the characteristics of chars during devolatilization in oxy-steam combustion process, Appl. Energy 182 (2016) 20–28, https://doi.org/10.1016/j.apenergy.2016.08.121.
[11] Q. Mengxia, S. Sheng, G. Jian, S. Zhijun, X. Kai, X. Jun, H. Song, W. Yi, X. Jun, Effects of CO2/H2O on the characteristics of chars prepared in CO2/H2O/N2 atmospheres, Fuel Process. Technol. 173 (2018) 262–269, https://doi.org/10.1016/j.fuproc.2018.01.003.
[12] C. Dueso, M.C. Mayoral, J.M. Andrés, A.I. Escudero, L.I. Díez, Towards oxy-steam combustion: The effect of increasing the steam concentration on coal reactivity, Fuel 239 (2019) 534–546, https://doi.org/10.1016/j.fuel.2018.11.035.
[13] Z. Mao, L. Zhang, X. Zhu, C. Pan, B. Yi, C. Zheng, Modeling of an oxy-coal flame under a steam-rich atmosphere, Appl. Energy 161 (2016) 112–123, https://doi.org/10.1016/j.apenergy.2015.10.018.
[14] C. Bu, A. Gómez-Barea, B. Leckner, X. Wang, J. Zhang, G. Piao, The effect of H2O on the oxy-fuel combustion of a bituminous coal char particle in a fluidized bed: Experiment and modeling, Combust. Flame 218 (2020) 42–56, https://doi.org/10.1016/j.combustflame.2020.03.025.
[15] S. Seepana, S. Jayanti, Steam-moderated oxy-fuel combustion, Energy Convers. Manage. 51 (10) (2010) 1981–1988, https://doi.org/10.1016/j.enconman.2010.02.031.
[16] L. Li, L. Duan, S. Tong, E.J. Anthony, Combustion characteristics of lignite char in a fluidized bed under O2/N2, O2/CO2 and O2/H2O atmospheres, Fuel Process. Technol. 186 (2019) 8–17, https://doi.org/10.1016/j.fuproc.2018.12.007.
[17] H.-L. Tay, S. Kajitani, S. Zhang, C.-Z. Li, Effects of gasifying agent on the evolution of char structure during the gasification of Victorian brown coal, Fuel 103 (2013) 22–28, https://doi.org/10.1016/j.fuel.2011.02.044.
[18] B. Yi, L. Zhang, F. Huang, Z. Mao, C. Zheng, Effect of H2O on the combustion characteristics of pulverized coal in O2/CO2 atmosphere, Appl. Energy 132 (2014) 349–357, https://doi.org/10.1016/j.apenergy.2014.07.031.
[19] M. Qing, S. Su, H. Chi, J. Xu, Z. Sun, J. Gao, K. Xu, S. Hu, Y. Wang, X. Hu, J. Xiang, Relationships between structural features and reactivities of coal-chars prepared in CO2 and H2O atmospheres, Fuel 258 (2019), 116087, https://doi.org/10.1016/j.fuel.2019.116087.
[20] G. Goetz, N. Nsakala, R. Patel, T. Lao, Combustion and Gasification Characteristics of Four Commercially Significant Coals of Different Rank, Report No, AP-261, EPRI (1982) 145.
[21] M.D. Mann, R.Z. Knutson, J. Erjavec, J.P. Jacobsen, Modeling reaction kinetics of steam gasification for a transport gasifier, Fuel 83 (11) (2004) 1643–1650, https://doi.org/10.1016/j.fuel.2004.02.002.
[22] D.G. Roberts, D.J. Harris, Char Gasification with O2, CO2, and H2O: Effects of Pressure on Intrinsic Reaction Kinetics, Energy Fuels 14 (2) (2000) 483–489, https://doi.org/10.1021/ef9901894.
[23] H. Liu, H. Zhu, M. Kaneko, S. Kato, T. Kojima, High-Temperature Gasification Reactivity with Steam of Coal Chars Derived under Various Pyrolysis Conditions in a Fluidized Bed, Energy Fuels 24 (1) (2010) 68–75, https://doi.org/10.1021/ef9004994.
[24] W.F. DeGroot, G.N. Richards, Relative rates of carbon gasification in oxygen, steam and carbon dioxide, Carbon 27 (2) (1989) 247–252, https://doi.org/10.1016/0008-6223(89)90130-9.
[25] D.G. Roberts, D.J. Harris, Char gasification in mixtures of CO2 and H2O: Competition and inhibition, Fuel 86 (17) (2007) 2672–2678, https://doi.org/10.1016/j.fuel.2007.03.019.
[26] C. Chen, J. Wang, W. Liu, S. Zhang, J. Yin, G. Luo, H. Yao, Effect of pyrolysis conditions on the char gasification with mixtures of CO2 and H2O, Proc. Combust. Inst. 34 (2) (2013) 2453–2460, https://doi.org/10.1016/j.proci.2012.07.068.
[27] R.C. Everson, H.W.J.P. Neomagus, H. Kasaini, D. Njapha, Reaction kinetics of pulverized coal-chars derived from inertinite-rich coal discards: Gasification with carbon dioxide and steam, Fuel 85 (7) (2006) 1076–1082, https://doi.org/10.1016/j.fuel.2005.10.016.
[28] C. Guizani, F.J. Escudero Sanz, S. Salvador, The gasification reactivity of high-heating-rate chars in single and mixed atmospheres of H2O and CO2, Fuel 108 (2013) 812–823, https://doi.org/10.1016/j.fuel.2013.02.027.
[29] J.F. Strange, P.L. Walker, Carbon-carbon dioxide reaction: Langmuir-Hinshelwood kinetics at intermediate pressures, Carbon 14 (6) (1976) 345–350, https://doi.org/10.1016/0008-6223(76)90008-7.
[30] F. Vallejos-Burgos, N. Díaz-Pérez, Á. Silva-Villalobos, R. Jiménez, X. García, L. R. Radovic, On the structural and reactivity differences between biomass- and coal-derived chars, Carbon 109 (2016) 253–263, https://doi.org/10.1016/j.carbon.2016.08.012.
[31] G.M. Meconi, R. Zangi, Adsorption-induced clustering of CO2 on graphene, PCCP 22 (37) (2020) 21031–21041, https://doi.org/10.1039/D0CP03482G.
[32] R. Akilan, M. Malarkodi, S. Vijayakumar, S. Gopalakrishnan, R. Shankar, Modeling of 2-D hydrogen-edge capped defected & boron-doped defected graphene sheets for the adsorption of CO2, SO2 towards energy harvesting applications, Appl. Surf. Sci. 463 (2019) 596–609, https://doi.org/10.1016/j.apsusc.2018.08.179.
[33] V.O. Özçelik, S. Cahangirov, S. Ciraci, Stable Single-Layer Honeycomblike Structure of Silica, Phys. Rev. Lett. 112 (24) (2014), 246803, https://doi.org/10.1103/PhysRevLett.112.246803.
[34] N. Osouleddini, S.F. Rastegar, DFT study of the CO2 and CH4 assisted adsorption on the surface of graphene, J. Electron Spectrosc. Relat. Phenom. 232 (2019) 105–110, https://doi.org/10.1016/j.elspec.2018.11.006.
[35] A.M. Oyarzún, X. García-Carmona, L.R. Radovic, Kinetics of oxygen transfer reactions on the graphene surface. Part II. H2O vs. CO2, Carbon 164 (2020) 85-99. 10.1016/j.carbon.2020.01.011.
[36] D. Zhao, H. Liu, P. Lu, H. Yu, M. Qin, A DFT study of the mechanism of H transfer during steam gasification, Combust. Flame 219 (2020) 327–338, https://doi.org/10.1016/j.combustflame.2020.06.006.
[37] K. Li, R. Khanna, H. Zhang, S. Ma, Z. Liang, G. Li, M. Barati, J. Zhang, Thermal behaviour during initial stages of graphene oxidation: Implications for reaction kinetics and mechanisms, Chem. Eng. J. 421 (2021), 129742, https://doi.org/10.1016/j.cej.2021.129742.
[38] K. Li, R. Khanna, H. Zhang, A. Conejo, S. Ma, Z. Liang, G. Li, M. Barati, J. Zhang, Thermal behaviour, kinetics and mechanisms of CO2 interactions with graphene: An atomic scale reactive molecular dynamic study, Chem. Eng. J. 425 (2021), 131529, https://doi.org/10.1016/j.cej.2021.131529.
[39] S. Plimpton, Fast Parallel Algorithms for Short-Range Molecular Dynamics, J. Comput. Phys. 1 (117) (1995) 1–19.
[40] J. Chen, X. Pan, H. Li, H. Jin, J. Fan, Molecular dynamics investigation on supercritical water oxidation of a coal particle, J. Anal. Appl. Pyrol. 159 (2021), 105291, https://doi.org/10.1016/j.jaap.2021.105291.
[41] K. Chenoweth, A.C.T. van Duin, W.A. Goddard, ReaxFF Reactive Force Field for Molecular Dynamics Simulations of Hydrocarbon Oxidation, J. Phys. Chem. A 112 (5) (2008) 1040–1053, https://doi.org/10.1021/jp709896w.
[42] A.C.T. van Duin, S. Dasgupta, F. Lorant, W.A. Goddard, ReaxFF: A Reactive Force Field for Hydrocarbons, J. Phys. Chem. A 105 (41) (2001) 9396–9409, https://doi.org/10.1021/jp004368u.
[43] F. Castro-Marcano, A.M. Kamat, M.F. Russo, A.C.T. van Duin, J.P. Mathews, Combustion of an Illinois No. 6 coal char simulated using an atomistic char representation and the ReaxFF reactive force field, Combust. Flame 159(3) (2012) 1272-1285. 10.1016/j.combustflame.2011.10.022.
[44] M.R. Weismiller, A.C.T. van Duin, J. Lee, R.A. Yetter, ReaxFF Reactive Force Field Development and Applications for Molecular Dynamics Simulations of Ammonia Borane Dehydrogenation and Combustion, J. Phys. Chem. A 114 (17) (2010) 5485–5492, https://doi.org/10.1021/jp100136c.
[45] K.M. Bal, E.C. Neyts, Direct observation of realistic-temperature fuel combustion mechanisms in atomistic simulations, Chem. Sci. 7 (8) (2016) 5280–5286, https://doi.org/10.1039/C6SC00498A.
[46] D. Hong, T. Si, X. Li, X. Guo, Reactive molecular dynamic simulations of the CO2 gasification effect on the oxy-fuel combustion of Zhundong coal char, Fuel Process. Technol. 199 (2020), 106305, https://doi.org/10.1016/j.fuproc.2019.106305.
[47] M.F. Irfan, M.R. Usman, K. Kusakabe, Coal gasification in CO2 atmosphere and its kinetics since 1948: A brief review, Energy 36 (1) (2011) 12–40, https://doi.org/10.1016/j.energy.2010.10.034.
[48] Heterogeneous Solid State Reactions, Chemical Kinetics of Solids1995, pp. 137-164. 10.1002/9783527615537.ch06.
[49] K. Li, J. Zhang, Z. Liu, X. Ning, T. Wang, Gasification of Graphite and Coke in Carbon-Carbon Dioxide–Sodium or Potassium Carbonate Systems, Ind. Eng. Chem. Res. 53 (14) (2014) 5737–5748, https://doi.org/10.1021/ie4039955.

[50] V.M. Gorbachev, Remarks on the application of the combined Kolmogorov — Erofeev — Kazeev — Avrami — Mampel equation in the kinetics of non-isothermal transformations, J. Therm. Anal. Calorim. 13 (3) (1978) 509–514, https://doi.org/10.1007/bf01912390.
[51] K.A. Connors, Chemical Kinetics: The Study of Reaction Rates in Solution, VCH1990.
[52] A.M. Oyarzún-Aravena, C. Gottschalk-Ojeda, I. Moya-Barría, F. Vallejos-Burgos, Edge type effect in the gasification mechanism of graphene clusters with H_2O and/or CO_2: armchair vs. zigzag, Carbon 193 (2022) 412-427. 10.1016/j.carbon.2022.02.048.
[53] M.K. Jena, V. Kumar, S. Liu, H. Vuthaluru, Steam gasification of low-rank coal chars: Insights into the kinetic compensation effects and physical significance of kinetic parameters, Chem. Eng. J. Adv. 11 (2022), 100306, https://doi.org/10.1016/j.ceja.2022.100306.
[54] S. Saqline, Z.Y. Chua, W. Liu, Coupling chemical looping combustion of solid fuels with advanced steam cycles for CO2 capture: A process modelling study, Energy Convers. Manage. 244 (2021), 114455, https://doi.org/10.1016/j.enconman.2021.114455.
[55] J. Kim, H. Choi, J. Lim, Y. Rhim, D. Chun, S. Kim, S. Lee, J. Yoo, Hydrogen production via steam gasification of ash free coals, Int. J. Hydrogen Energy 38 (14) (2013) 6014–6020, https://doi.org/10.1016/j.ijhydene.2012.12.058.
[56] V. Kyriakou, I. Garagounis, A. Vourros, G.E. Marnellos, M. Stoukides, A protonic ceramic membrane reactor for the production of hydrogen from coal steam gasification, J. Membr. Sci. 553 (2018) 163–170, https://doi.org/10.1016/j.memsci.2018.02.047.
[57] R. Roncancio, J.P. Gore, CO2 char gasification: A systematic review from 2014 to 2020, Energy Convers. Manage.: X 10 (2021), 100060, https://doi.org/10.1016/j.ecmx.2020.100060.
[58] M. Obersteiner, C. Azar, P. Kauppi, K. Möllersten, J. Moreira, S. Nilsson, P. Read, K. Riahi, B. Schlamadinger, Y. Yamagata, J. Yan, J.-P.v. Ypersele, Managing Climate Risk, Science 294(5543) (2001) 786-787. 10.1126/science.294.5543.786b.
[59] Callide Oxyfuel Project. https://www.csenergy.com.au/what-we-do/generating-energy/callide-power-station/callide-oxyfuel-project.